論文 / 著書情報
Article / Book Information

Title	Centrifugal tests on minimization of flood-induced deformation of levees by steel drainage pipes
Authors	Jenisha Singh, Kazuki Horikoshi, Yusuke Mochida, Akihiro Takahashi
Citation	Soils and Foundations, Vol. 59, Issue 2, pp. 367-379
Pub. date	2019, 4

HOSTED BY
ELSEVIER
Available online at www.sciencedirect.com
ScienceDirect
Soils and Foundations 59 (2019) 367–379
www.elsevier.com/locate/sandf

Centrifugal tests on minimization of flood-induced deformation of levees by steel drainage pipes

Jenisha Singh [a], Kazuki Horikoshi [a], Yusuke Mochida [b], Akihiro Takahashi [a,*]

[a] Department of Civil and Environmental Engineering, Tokyo Institute of Technology, 2-12-1 O-okayama, Tokyo 152-8552, Japan
[b] Nippon Steel & Sumitomo Metal Corporation Research & Development, 20-1 Shintomi, Futtsu, Chiba 293-8511, Japan

Received 20 March 2018; received in revised form 25 October 2018; accepted 3 December 2018
Available online 5 February 2019

Abstract

The rise in the river water level in a levee raises the phreatic surface. This facilitates the development of positive pore water pressure in the region below the phreatic surface, and consequently, reduces the shear strength of the soil. Steel drainage pipes that can provide both drainage and reinforcement functions could be a better option for levee protection against flooding compared to the traditional method of protection which can provide only one or the other of these functions. This paper presents the results of a series of centrifugal tests for six cases conducted to investigate the effectiveness of newly designed steel drainage pipes for minimizing the flood-induced deformation of levees. The test results reveal that the installation of these steel drainage pipes (1) allows the levee to withstand a higher flood water head and extended flood duration and (2) is effective for limiting the continuation of the slip line in the slope. The quick drainage of the seepage water can restrict the development of positive pore water pressure in the slope, and the mobilization of the axial force in the pipes minimizes the flood-induced deformation of the levee.

Keywords: Levee; Seepage; Centrifuge modeling; Drainage; Reinforcement; Steel pipe

1. Introduction

Increased seepage flow in levees during a flood can cause destabilization by an increase in the self-weight of the soil and a reduction in shear strength due to the decrease in effective stress by the reduction in matric suction (Chu-Agor et al., 2008; Polemio and Lollino, 2011; Schnellmann et al., 2010; Vanapalli et al., 1996; Vandamme and Zou, 2013). A reduction in the soil strength in a slope brought about by the decrease in effective stress can cause soil mass movement, making the slope unstable (Hamdhan and Schweiger, 2011; Krahn et al., 1989; Ling et al., 2009; Ng et al., 2003; Timpong et al., 2007). Additional protective measures in levees subjected to seepage flow could enhance the level of safety against seepage-induced failure. This additional protection can be provided in the form of drainage, which would limit the rise in the phreatic surface, or in the form of reinforcement, which would compensate for the loss in shear strength caused by the seepage flow through the mobilization of additional strength.

Drainage pipes are one of the standard methods of protection, used mostly in existing levees, to limit the decrease in effective stress by limiting the development of positive pressure (Choi, 1984; Rahardjo et al., 2011, 2003; Resnick and Znidarcic, 1990). However, drainage pipes also have some limitations in terms of protecting levees, namely, their performance is affected by the hydraulic

Peer review under responsibility of The Japanese Geotechnical Society.
* Corresponding author.
E-mail addresses: singh.j.aa@m.titech.ac.jp (J. Singh), horikoshi.k.aa@m.titech.ac.jp (K. Horikoshi), mochida.8md.yuusuke@jp.nssmc.com (Y. Mochida), takahashi.a.al@m.titech.ac.jp (A. Takahashi).

https://doi.org/10.1016/j.sandf.2018.12.008
0038-0806/

properties of the soil, they cannot increase the performance beyond the critical length of the drainage, and they have a limited zone of influence (Cai et al., 1998; Chen and Chen, 2016; Ghiassian and Ghareh, 2008). Soil nails are another protective measure used in slope stability problems by the mobilization of additional strength. Soil nails, predominantly through the development of axial force, increase the shear resistance in the slope (Allersma and Bartsch, 2004; Cai and Ugai, 2003; Tei et al., 1998; Zhang et al., 2001). Ng et al. (2006) and Rotte and Viswanadham (2012), with series of the centrifuge experiments, and Li et al. (2008) and Zhou et al. (2009), with full-scale tests, confirmed the effectiveness of soil nails in the global stability of slopes subjected to seepage flow. In their studies, however, the limitation of the soil nail performance was also shown, as soil nails are only capable of minimizing the formation of cracks and local failure, but cannot prevent them. Thus, protective measures for slopes that can only provide either drainage or reinforcement show their limitation when subjected to seepage flow. Combining both functions of drainage and an increase in reinforcement could provide a better solution to seepage-induced failure. In this study, therefore, the possibility of using steel drainage pipes in levees for protection against seepage-induced failure is investigated through a series of centrifugal tests. Steel drainage pipes comprise a newly designed protective measure which is capable of providing both functions of drainage and reinforcement. Steel drainage pipes can provide this dual function because their design calls for a tubular structure with numerous holes on the surface and a spiral blade at one end.

2. Experimental program

A series of centrifugal tests for six different cases is performed using the Tokyo Tech Mark III centrifuge (Takemura et al., 1999) at the centrifugal acceleration of 20*g*. The model ground and the testing conditions are determined following the common centrifuge scaling law, in which the model ground is scaled down so that the same stress condition as in the prototype ground is achieved when subjected to centrifugal acceleration. One of the reasons for using the centrifuge modelling is that the tests involve the wetting process of the soil and that the relatively high capillary rise, commonly seen in scaled-down physical model tests, is not preferred. To model the drainage pipes, dimensionally similar model pipes are used as they can provide proportional drainage capacity in the model ground. The scaling law used for the centrifuge tests is summarised in Table 1. For all the test cases, a half section of a river levee with a side slope of 1H:1V is employed. The slope inclination is finalized after various trial centrifugal experiments and analysis were performed on the model with side slopes of 2H:1V, 1.6H:1V, 1.5H:1V, and 1H:1V for its ability to balance the stability before flooding and its vulnerability to failure. These trial experiments and results, however, are not included in this discussion. The designed levee might not represent the general levee configuration. However, the configuration allows for the development of failure when subjected to flooding during the tests. It should be noted that the designed model slope could not model the weak zone created by various factors such as, but not limited to, inhomogeneity which makes the levees vulnerable to seepage-induced failure. Hence, a steep slope was required to create failure in the tests. A similar slope inclination was also used by other researchers (Mori et al., 2012, 2011; Resnick and Znidarcic, 1990; Saghaee et al., 2017, 2016) for investigating the failure of levees/embankments subjected to seepage flow. Unless otherwise mentioned, the model configurations and test results in the following sections and figures are presented and discussed in the prototype scale.

Table 1
Scaling law for centrifuge tests (Cargill and Ko, 1983; Thusyanthan and Madabhushi, 2003).

Parameters	Ratio of model to prototype
Length	1/N
Area	$1/N^2$
Volume	$1/N^3$
Velocity	N
Pressure	1
Head	1/N
Intrinsic permeability	1
Time	$1/N^2$
Force	$1/N^2$
Bending moment	$1/N^3$

2.1. Material properties

Edosaki sand is used in the preparation of the model. The properties of Edosaki sand are tabulated in Table 2. The material is classified as silty sand (SM) according to the USCS. The foundation and the embankment are prepared with soil at a degree of compaction (Dc) of 95% (1.72 Mg/m^3) and a maximum dry density of 80% (1.45 Mg/m^3), respectively, determined from the Standard Proctor Compaction test. The soil water characteristic curve (SWCC) for the embankment and the principal parameters for the van Genuchten model are shown in Fig. 1. The surface layer on the slope is prepared by soil mixed with fibre to replicate the grass cover often found in real levees and to prevent the occurrence of unrealistic surface erosion during the experiment. The content of the fibre is 1% (for Cases 1–4, see the following subsection for details) or 2% (for Cases 5 and 6) of the dry weight of sand. The polyester fibre used in the tests, called Teijin RA04FN, was approximately 39 μm in diameter and 5 mm in length.

Steel drainage pipes, steel pipes filled with glue, and flexible pipes made of silicone are used for the different test cases as protection in the levee against seepage-induced deformation (to be described later). Fig. 2 shows the

Table 2
Properties of Edosaki sand.

Soil properties	Values
D_{50} (mm)	0.30
D_{10} (mm)	0.010
Coefficient of uniformity	38
Coefficient of gradation	8.53
Soil particle density (Mg/m^3)	2.72
Optimum moisture content	14.5%
Average initial water content of model ground	14.7%
Angle of shearing resistance [Degree of compaction Dc = 80%] (degrees)	
Soil without fiber	29
Soil with 1% fiber	31
Soil with 2% fiber	33
Cohesion [Dc = 80%](kN/m^2)	
Soil without fiber	2.5
Soil with 1% fiber	4.2
Soil with 2% fiber	6.0
Saturated coefficient of permeability (m/s)	
Foundation	1.5E−6
Embankment	4.5E−5
Dry density of embankment (Mg/m^3)	1.45
Dry density of foundation (Mg/m^3)	1.72

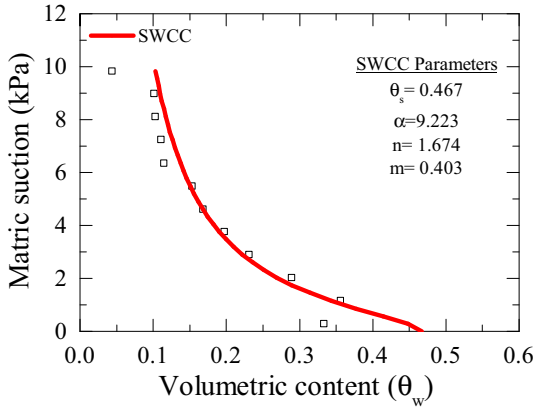

Fig. 1. Soil water characteristic curve (SWCC) for embankment.

dimensions of a steel drainage pipe in the prototype scale. The longitudinal section of the pipe with the spacing of the drainage holes, the spiral blade, and the locations of the strain gauges are shown in Fig. 2(a). Fig. 2(b) and (c) show the cross-sections of the steel drainage pipe and the steel pipe with only reinforcement, respectively. The steel drainage pipes are tubular. They have holes on the surface with a diameter of 24 mm and the spacing of 0.16 m. The end one-meter length of each pipe is provided with a spiral blade having an external diameter 0.16 m. The spiral blade provides better anchorage of the pipes to the soil. These pipes provide both drainage and reinforcement functions. Tubular steel pipes with the same configuration and material, but filled with glue (Shin-Etsu RE45T), are used to model the steel pipes with only the reinforcement function. The added glue in the pipes increases the overall weight of the pipes; however, only the reinforcement pipes which are mostly solid are expected to have a larger weight than the drainage pipes. Flexible silicone tubes (Young's modulus = 5.0E7 N/m^2) with the same internal dimension as the steel drainage pipes (keeping the drainage capacity similar), but without a spiral blade, are used to model the pipes with the drainage function. The external dimension of the drainage pipes, however, is 100 mm compared to 80 mm of the steel drainage pipes. This difference in external dimension is not expected to cause a significant difference in behaviour. These pipes could easily be bent and are not expected to provide significant additional reinforcement. The properties of the steel drainage pipes used in the experiments in the prototype scale are summarized in Table 3.

2.2. Test conditions

Six different cases of varying levels of protection are investigated in the study. Fig. 3 shows the geometry of the model slope and the arrangement of the pipes in the centrifuge models (Cases 1–6). The model slope consists of a 2-m-thick foundation layer and a 4-m-high embankment with a 1H:1V slope. The total length of the model ground is 12 m, and the width of the model is 3 m. Fig. 3 (a) shows the cross-section of the model with pipes. In Cases 2–6, the pipes are installed at a height of 1 m from the toe of the slope. Fig. 3(b) shows the arrangement of the pipes in the plan view for Cases 2–4 and 6. In all these cases, the slope is provided with three pipes. The pipes are installed at the spacing of 1 m. Steel pipes are used in Cases 2–4, whereas flexible silicone pipes are used in Case 6. In Case 5, two pipes are installed at the spacing of 2 m, as shown in Fig. 3(c). In all the cases, a surface layer of 0.2 m, made of soil mixed with fibre, is provided on the slope. The test conditions are summarized in Table 4. These cases are designed to study the effectiveness of the steel drainage pipes in slope stabilization as well as to understand the contribution of the drainage function and the reinforcement function separately.

2.3. Model preparation

All models are constructed in a container with inner dimensions of 1.4 × 3.0 × 9.0 m in the prototype scale and equipped with a transparent acrylic window. The container is divided into three sections, namely, an upstream supply section, a model section, and a downstream drainage section. The supply section and the drainage section both have a width of 1 m, while the model section has a width of 12 m in the prototype scale. A special arrangement of the acrylic plate is made in the container to prevent the channelization of the flow along the interface between the container wall and the model ground. In the model section, the 1:20 scaled-down model ground was prepared by dynamic compaction and an excavation technique. At first, the ground with a uniform cross-section of 11.4 × 3 × 6 m in the prototype scale is prepared by placing and compacting Edosaki sand in 12 layers. Using temporary supports,

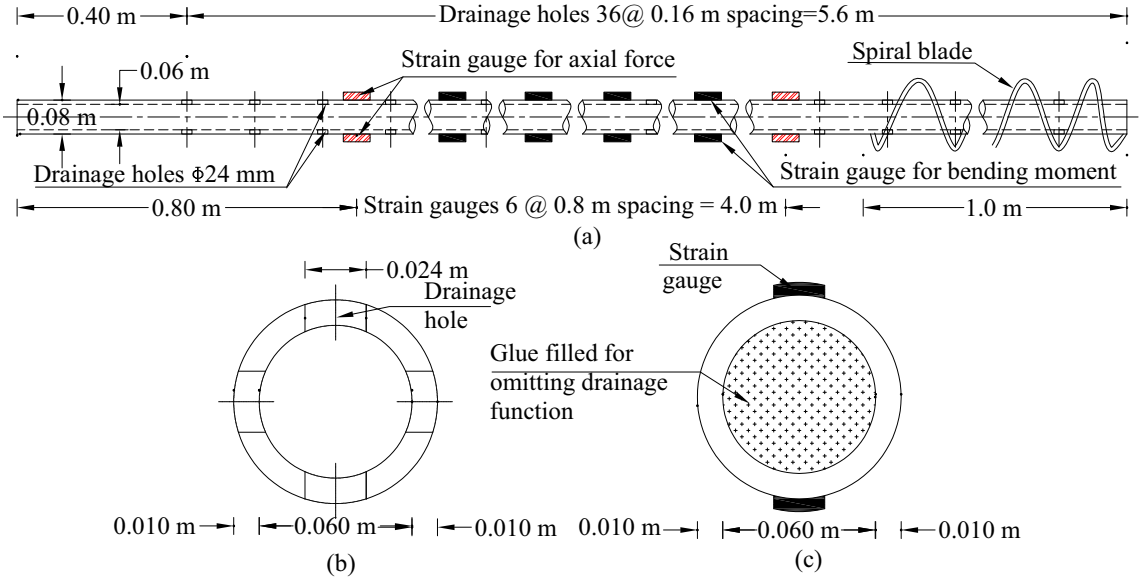

Fig. 2. Steel drainage pipe (a) longitudinal section with locations of strain gauges and drainage holes; (b) cross-section of steel drainage pipe (c) cross-section of only reinforcement pipe with strain gauge.

Table 3
Properties of steel drainage pipes.

Parameters	Values
Internal diameter (mm)	60
External diameter (mm)	80
Length (m)	6
Pitch of screw (mm)	160
Thickness of plate forming screw (mm)	20
External diameter of screw part (mm)	160
Young's modulus, E (N/m^2)	2.10E + 11
Poisson's ratio, v	0.3

each layer is compacted to have an equal thickness of 0.5 m to the target density and an average moisture content of 14.7% which is close to the optimum moisture content of the soil. The soil layers are compacted using a hand-held vibrator over the flat acrylic plate. While preparing the model ground, miniature pore water pressure transducers (PPTs), each with a wire mesh head [Model: SSK Micro Pressure Transducer P306V-02], are also placed in predetermined locations (locations A, B, C, and D in Fig. 3) with

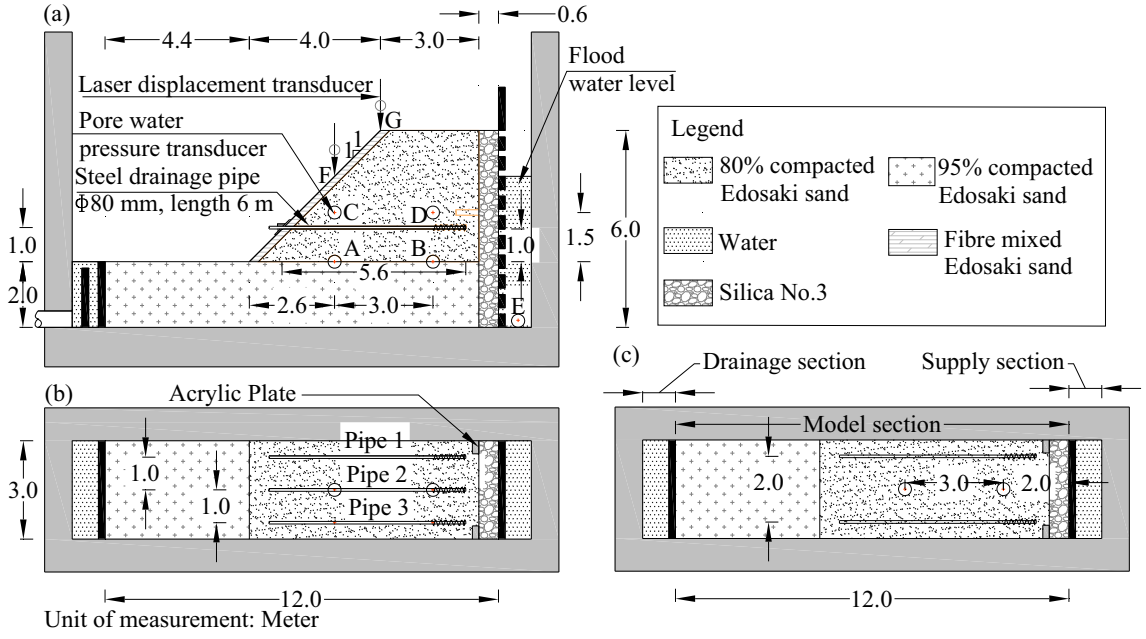

Fig. 3. Model Configuration (a) sectional view with geometry and location of sensors (b) plan view for Case 2–4, 6 (c) plan view for Case 5.

Table 4
Protection conditions in models.

Cases	Level of protection	Description of protection					
		Pipe 1		Pipe 2		Pipe 3	
		R	D	R	D	R	D
Case 1	Unreinforced	N/A	N/A	N/A	N/A	N/A	N/A
Case 2	Reinforced (3 steel drainage pipes)	○	○	○	○	○	○
Case 3	Reinforced (2 steel drainage pipes + 1 steel pipe)	○	○	○[a]	×	○	○
Case 4	Reinforced (3 steel pipes)	○	×	○[a]	×	○	×
Case 5	Reinforced (2 steel drainage pipes)	○	○	N/A	N/A	○	○
Case 6	Reinforced (3 drainage pipes)	×	○	×	○	×	○

Note: R = reinforcement function, pipes are made of steel; D = drainage function, pipes are tubular with holes on surface; ○ = present; × = not present; N/A = not available, pipes are not used; a = with strain gauges to measure axial force and bending moment.

precise measurement. After making the uniform model ground with Edosaki sand, a layer of silica sand No. 3, $0.6 \times 3 \times 6$ m (prototype scale), is prepared by pouring the sand into the gap between the Edosaki ground and the supply tank, resulting in a model ground with dimensions of $12 \times 3 \times 6$ m in the prototype scale. The model ground is then excavated to the designed configuration by placing the acrylic guide, having the same dimensions as the embankment, over the container and using a T-shaped blade.

The slope portion of the model is then further excavated resulting in a slope 0.2 m deeper than the required dimension. The layer of Edosaki sand mixed with fibre is compacted on the excavated slope surface with a degree of compaction of 80% to form the required model geometry. Two laser displacement transducers (LDTs) are used to measure the settlement at locations F and G (see Fig. 3 (a). Both LDTs have a sensor head of the LB-02 series manufactured by Keyence. However, two types of amplifiers are used here, LB60 series and LB62 series, with the measurement range of ±40 mm and ±10 mm, respectively. Marked noodles are placed on the side face of the model for the visual observation of the deformation pattern through the transparent window. Apart from this, in Cases 3 and 4, the central pipe (Pipe 2 in Fig. 3(b)) is equipped with strain gauges to measure the axial force with axial force sensors at two locations (sensors give the average strain value of the strain gauges placed on the top and the bottom of the pipe) and to measure the bending moment with bending moment sensors at four locations (sensors give the difference in strain values of the strain gauges placed on the top and the bottom of the pipe). The wires of these sensors are passed through the inside of the pipes to prevent the channelization of flow that would occur if they were present on the surface of the pipes.

In Cases 2–6, the steel pipes/drainage pipes are driven at each specified location using the acrylic guide after making a hole with an auger drill bit. The embedment length is kept at 5.6 m for all the pipes. After the pipes are equipped, aluminum facing plates with the dimensions of $0.6 \times 0.6 \times 0.04$ m are installed and fixed with acrylic caps. Water is supplied to the supply section and collected from the drainage section through the pipe connection. The drained water is then collected in a separate drainage tank. Additional PPTs are installed in the supply section of the container and the drainage tank for measuring the supply flood water head and the amount of drainage water, respectively. For visual observations of the slope during the test, two high-definition video recorders (top and side) along with one high-resolution digital camera (side) are used.

2.4. Testing procedure

After the set-up has been completed, saturation of the foundation layer is carried out. For saturation, de-aired water is supplied to the supply section until the volume of water exceeds the calculated volume of the pores of the foundation layer. At this stage, the apparent water level in the model is slightly higher than the top of the foundation. After the completion of saturation of the foundation at 1*g*, centrifugal acceleration is increased in steps to the target 20*g*. After the centrifugal acceleration has reached 20*g*, the steady state is ensured by allowing the pore water pressure measurement to become stable. At this stage, the water level in the model is near the top of the foundation and unaffected by the absence or presence of the protection. The phenomenon of a flood in a river channel is then simulated by raising the water level in the supply section as in the experiment conducted by Horikoshi and Takahashi (2015) and Koito et al. (2016). Fig. 4 shows the time histories of the flood water head supplied in the supply tank for the six cases. The flood water head is the difference between the supply water level and the drainage water level (equal to the top of the foundation). In Cases 1–4, the rising rate of the flood water is small, in the range of 0.03–0.06 m/hr, while in Cases 5 and 6, it is large, around 0.3 m/hr. This unintentional difference in rising rates does not allow for a direct comparison of the time reference among all the cases. In Cases 1–4, a steady state of the seepage flow is achieved, whereas in Cases 5 and 6, a steady state of the seepage flow is not achieved. Therefore, a comparison of Cases 1–4, where similar seepage conditions are achieved,

is done to understand the effectiveness of the steel drainage pipes, and a comparative performance of the steel drainage pipes with the pipes that only have the reinforcement function in slope protection is also made. A comparison of Cases 5 and 6 is done to understand the comparative performance of the steel drainage pipes with the dual function and the pipes with only the drainage function in slope protection. The water level is continuously monitored through the transducers' record and visual observations of the standpipe through the video camera records. The flow of water is controlled manually by a valve from the centrifuge control room.

3. Centrifugal test results

3.1. Effect of steel drainage pipes on propagation of sliding

The effectiveness of the steel drainage pipes on minimizing the propagation of the slip line and a comparative performance of the steel drainage pipes with pipes providing only the reinforcement function are investigated through a comparison of the reinforced cases (Cases 2–4) with the unreinforced case (Case 1). The comparative performance of the steel drainage pipes with pipes providing only the drainage function is investigated through a comparison of Cases 5 and 6. The deformation of the levee is evaluated by observations of the marked noodles through the transparent window and the measured displacements using the LVDTs.

Fig. 5 shows the superimposed images of the levee at the initial condition and after the seepage test for all the cases along with the initial shape, deformed shape, and slip line. The superimposed images show the overall performance of the model ground among the different cases under various levels of protection provided in the model ground. In Case 1, the failure starts from the toe region and progressively extends to the crest causing the complete collapse of the levee, i.e., the retrogressive failure mode occurs (Wang and Sassa, 2003), as shown in Fig. 5(a). In Cases 2 and 5, with the presence of the steel drainage pipes, seepage-induced failure is prevented, as shown in Fig. 5(b) and (e), respectively. In Case 3, even though the levee suffered surface erosion below the location of the pipe before the seepage test (while increasing the centrifugal acceleration as the increasing rate of the centrifugal acceleration was rather large compared to the other cases), the large deformation of the levee is prevented. The surface erosion in Case 3 is attributed to the insufficient manual control over the rate of increase in centrifugal acceleration. The presence of erosion below the toe region before the seepage test facilitated the continuation of erosion, especially above Pipe 1 and Pipe 3 during the rise in flood water. Along with this, tension cracks are observed on the crest of the levee. However, significant movement of the soil mass is prevented, as shown in Fig. 5(c). In Case 4, for which protection of the levee is provided by steel pipes without the drainage function, the continuation of the slip line below the location of the pipe is stopped. However, the formation of deeper tension cracks on the crest and the consequent large deformation of the levee are not prevented, as shown in Fig. 5(d). In Case 6, for which protection of the levee is provided by flexible tubular pipes without the reinforcement function, the slip line continues from the toe to the crest of the levee. The progression of failure begins with the settlement of the pipe leading to the eventual large deformation of the levee, as shown in Fig. 5(f).

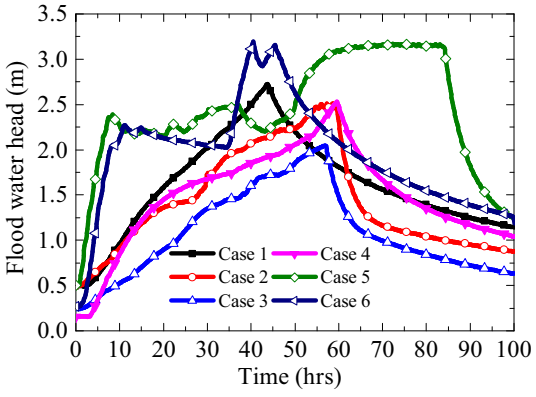

Fig. 4. Time histories of supply flood water head.

3.2. Effect of steel drainage pipes on resistance against flood

Fig. 6 shows the time histories of the settlement at location F (shown in Fig. 3) along with the indication of the flood head at the initiation of the movement represented by the numbers on the vertical line for Case 1 (unreinforced), Case 3 (both reinforcement and drainage), Case 4 (only reinforcement), and Case 6 (only drainage). In the figure, Cases 2 and 5 are not shown as no significant movement is observed in these cases. The results of the centrifugal tests with respect to the point of the initiation of failure (onset of the soil movement) and the occurrence of large failure (large deformation leading to a change in the geometry of the slope) are presented in Table 5.

The observations can be summarised as follows. In Cases 2 and 5, failure is completely prevented. In Case 3, a slight movement of the slope is observed with no large deformation of the slope. In all these cases (Cases 2, 3, and 5), protection of the levee is provided by the steel drainage pipes. In Case 4, a more extensive movement of the soil slope is observed; however, the large deformation of the slope that is observed in Case 1 is prevented. In Case 6, there is a large deformation of the slope compared to no significant deformation in Case 5.

Fig. 7(a) shows the changes in the pore water pressure at location A with the increasing flood head for Case 1 (unreinforced), Case 2 (both reinforcement and drainage), and Case 4 (only reinforcement), while Fig. 7(b) shows the same for Case 5 (both reinforcement and drainage) and Case 6 (only drainage). The vertical lines in the graph indicate the flood water head at which the failure is initiated. The

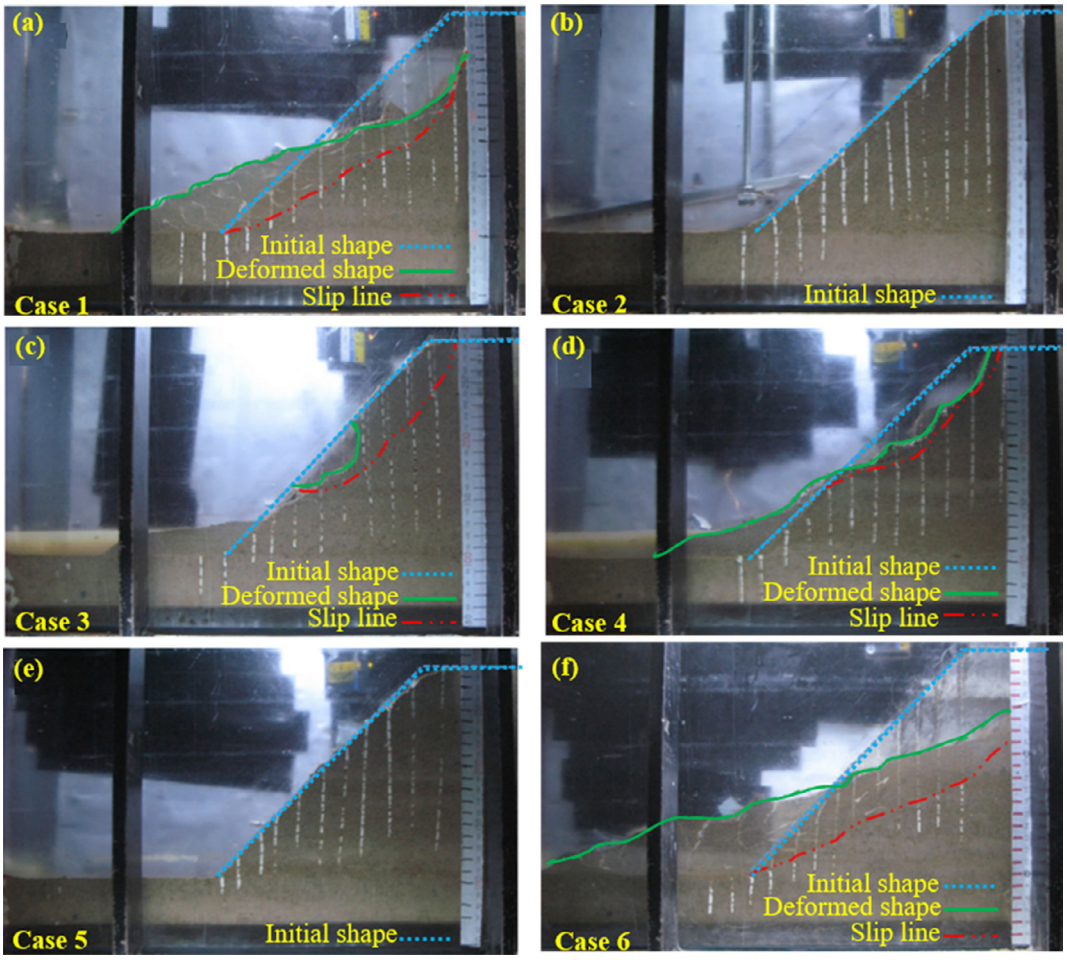

Fig. 5. Superimposed image of initial condition (before seepage test) of slope with deformed shape of slope after experiment (after test completion) (a) Case 1; (b) Case 2; (c) Case 3; (d) Case 4; (e) Case 5; (f) Case 6.

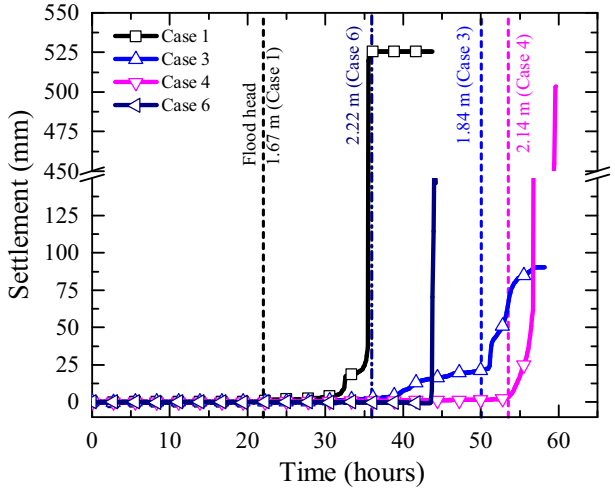

Fig. 6. Time histories of settlement on location F.

horizontal line indicates the pore water pressure at location A when the failure is initiated. In Fig. 7(a), it is observed that, in Case 1, failure occurs when the flood water head reaches 1.67 m and the pore water pressure reaches 10.6 kPa. In Case 4, failure starts when the pore water pressure at location A reaches 13.3 kPa and the flood water head reaches 2.14 m. These differences in pore water pressure, which indicate where the failure starts, show that the slope could withstand the development of larger positive pore water pressure and a higher flood water head with the reinforcement provided by the pipes. Fig. 7(b) shows the development of pore water pressure with the flood water head for Cases 5 and 6. In Case 6, failure is again initiated when the pore water pressure at location A reaches about 10.6 kPa, as in Case 1; however, to achieve this pore water pressure, a higher flood head of 2.22 m is required. It should also be taken into consideration that the failure in Case 6 starts when the flood water head has been maintained at this value (with the slight descending trend; see Fig. 4) for almost 20 h during the seepage test. The development of pore water pressure in Cases 5 and 6 follows a similar trend. However, no failure occurs in Case 5, highlighting the added protection provided by the dual function of the steel drainage pipes in Case 5. In Case 2, the pore water pressure is maintained at a lower level than the pore water pressure at the failure condition of other cases for a similar flood water head, thus preventing failure.

Table 5
Summary of centrifugal experiment results.

Cases	Initiation of failure		Occurrence of large failure	
	Seepage flow duration (h)	Flood head (m)	Seepage flow duration (h)	Flood head (m)
Case 1	22	1.67	35	2.2
Case 2	No failure			
Case 3	50	1.84	No large deformation	
Case 4	53.5	2.14	57 (no complete failure)	2.3
Case 5[b]	No failure			
Case 6[b]	36	2.22	43	2.9

Note: b = flood rising rate in these cases is different from other cases and direct comparison cannot be made in time reference.

4. Contribution of drainage and reinforcement in slope protection

4.1. Drainage contribution

The proposed steel drainage pipes, due to their tubular structure and numerous holes on the surface, enhance the drainage of the seepage water, and thus, limit the rise in the pore water pressure in the slope. Fig. 8 shows the variation in the discharge rate with the flood water head for Cases 1–6. The discharge rate here is calculated from the change in the level of water in the drainage tank measured by the PPTs. For cases where drainage through the pipes is available (Cases 2, 3, 5, and 6), the discharge rate is much larger than the cases without drainage (Cases 1 and 4). It should be noted that no substantial difference in the discharge rate is observed between the cases with three drainage pipes (Cases 2 and 6) and the cases with two drainage pipes (Cases 3 and 5). This may be due to (i) the large scatter in the estimated discharge rate and (ii) more than enough capacity of the drainage pipes. In the cases with drainage, a sharp rise in the discharge rate is observed when the flood head exceeds 1.5 m. Since the pipes are installed at a height of 1 m from the top of the foundation, the effectiveness of the pipes to drain the water is observed when the flood head is above the location of the pipes, as shown in Fig. 8.

Fig. 9 shows the changes in pore water pressure at locations A and B with the flood water head for all the cases along with the pore water pressure corresponding to the fully developed steady state seepage. To obtain the pore water pressure developing at the fully developed steady state seepage condition, a steady state seepage analysis is performed on the levee without drainage by varying the

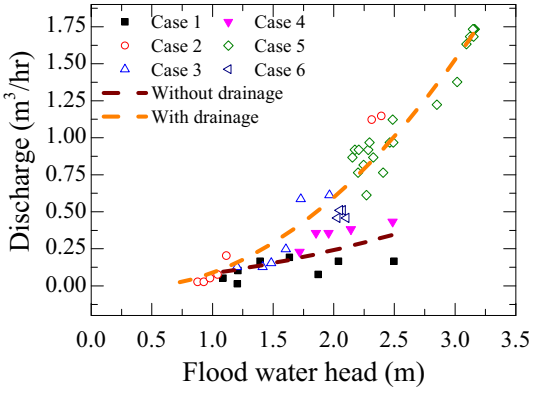

Fig. 8. Change in discharge rate with flood water head.

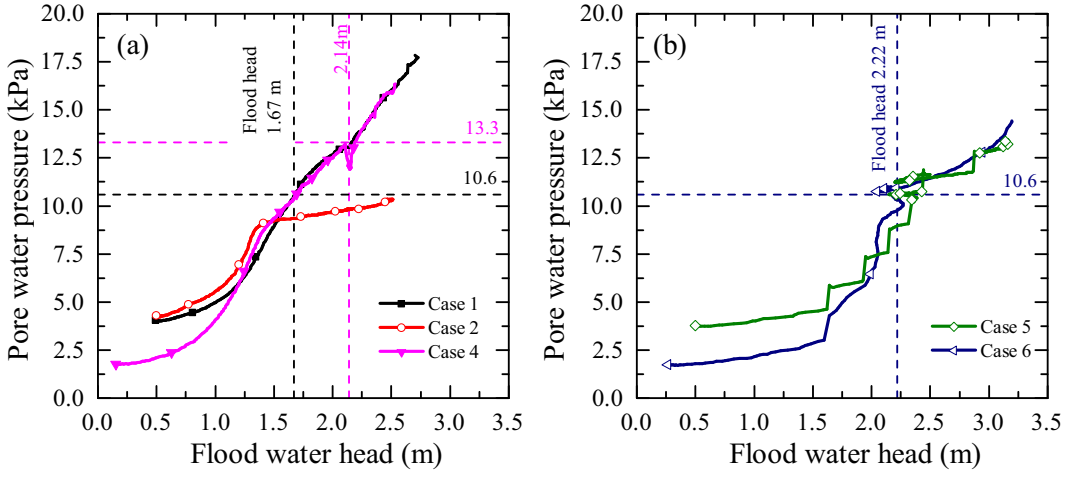

Fig. 7. Development of pore water pressure at location A (below slope) with flood water head (a) Case 1, 2 and 4; (b) Case 5 and Case 6.

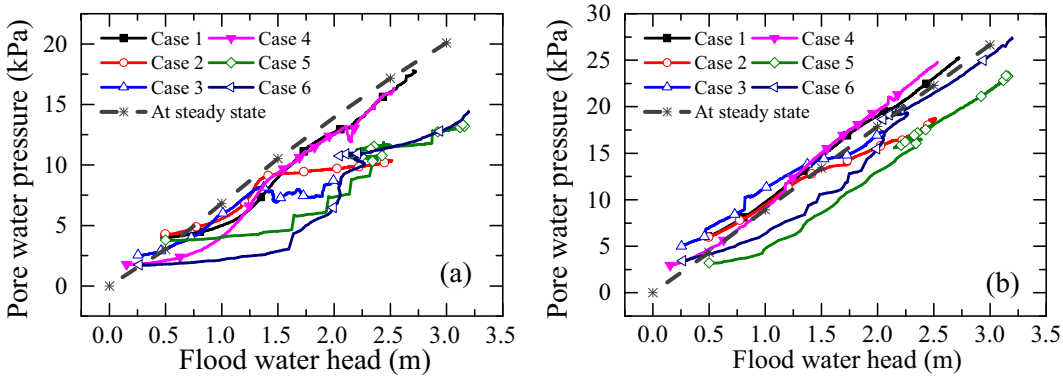

Fig. 9. Development of pore water pressure with flood water head (a) at location A (below slope); (b) at location B (below crest).

boundary condition (flood water level). In Fig. 9(a), a clear distinction in the variation in pore water pressure at location A is seen between the cases with drainage (Cases 2, 3, 5, and 6) and without drainage (Cases 1 and 4), as is observed in the variation in discharge rate with the flood water head. The rise in pore water pressure at location A is restricted in the cases with drainage. In the cases without drainage, the rise in pore water pressure follows a similar trend and monotonically increases with the flood water head and is similar to the pore water pressure corresponding to the steady state seepage flow. The increase in pore water pressure at location B with the rise in the flood water head is shown in Fig. 9(b). In Cases 1–4, the trend of the rise is similar in all cases regardless of the presence or absence of drainage and is also similar to the pore water pressure estimated by the steady state seepage analysis on the levee without drainage. From the graph, it can be observed that, in Cases 1–4, the steady state of the seepage flow is achieved, whereas in Cases 5 and 6, the pore water pressure development is below the steady state condition. Thus, with the drainage function in the pipes, the phreatic surface is lowered especially near the slope. The effectiveness of lowering the phreatic surface decreases along the length of the pipe. The limited rise in the pore water pressure near the slope prevents the large deformation of the slope in cases where the levee is provided with drainage in combination with reinforcement. In Fig. 9(a), it can be observed that the trend in the development of pore water pressure is very similar in Cases 5 and 6, indicating that the two pipes in Case 5 can meet the drainage requirement as sufficiently as the three pipes in Case 6. However, the level of the deformation in these cases is entirely different, as mentioned above. No significant deformation is observed in Case 5, whereas large deformation is observed in Case 6. This indicates that the levee provided with steel drainage pipes, having the combination of the drainage and reinforcement functions, experiences more superior protection than the levee provided with only the drainage function. Nonetheless, the drainage pipes are effective for restricting the build-up of pore water pressure near the slope surface, which is crucial for slope stability and increases the resilience against failure induced by the seepage flow.

4.2. Reinforcement contribution

Steel drainage pipes, by their stiffness and special spiral blade arrangement at the end of the pipe, can provide reinforcement when used in a levee. To understand the contribution of the reinforcement by the proposed steel drainage pipes, strain gauges are installed to measure the axial force and bending moment in the central pipe in Cases 3 and 4. Fig. 10(a)–(c) show the time histories of the flood-induced axial force near the facing plate (0.4 m from the

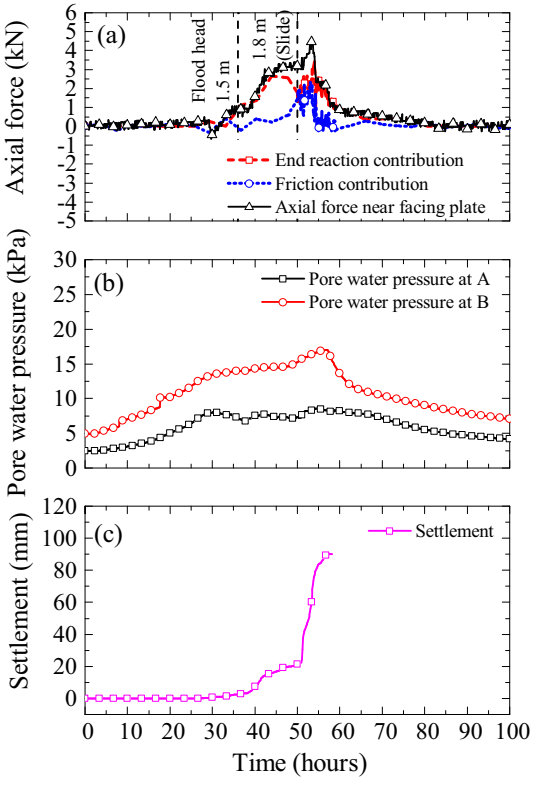

Fig. 10. Time histories of (a) axial force with its component (b) pore water pressure at location A and B (c) settlement at location F, in Case 3.

slope surface) along with its components, pore water pressure at locations A and B, and settlement at location F, respectively, for Case 3. The axial force is set to zero at the beginning of the seepage test. Therefore, the change in axial force is the result of the soil deformation caused by the seepage flow. Here, the positive value indicates the increase in tensile force and the negative value indicates the decrease in tensile force from the initial condition, i.e., at the onset of the seepage test. In Fig. 10(a), the vertical dotted lines indicate the time with the flood head at which the axial force is mobilized and sliding is observed in the experiment. The axial force is mobilized when the flood water head exceeds 1.5 m, i.e., it lies above the location of the pipe (after 30 h, see Fig. 4). This mobilization of the axial force provides the additional confinement to the soil in the shallower portion and contributes to the global stability of the slope. The axial force can be decomposed into the contribution of the end reaction (reaction at the spiral blade part) and the skin friction of the pipe surface and soil in the section without the spiral blade. The components of axial force for Case 3 are shown in Fig. 10(a). The end reaction here is the axial force measured 4.4 m from the slope surface, while the skin friction in the section without the spiral blade is estimated as the difference between the axial forces measured 0.4 m and 4.4 m from the slope surface. The pore water pressure, shown in Fig. 10(b), is measured near the points where the axial force is close to the facing plate, i.e., at location A and the end reaction, i.e., location B. The time history of the settlement is shown in Fig. 10(c); it is calculated by setting the settlement at the beginning of the rise of the flood water head to equal zero.

Similarly, Fig. 11(a)–(c) show the time histories of the flood-induced axial force near the facing plate (0.4 m from the slope surface) along with its component, the pore water pressure at locations A and B, and the settlement at location F, respectively, for Case 4. In Fig. 11(a), the vertical dotted lines indicate the time with the flood head at which the axial force is mobilized and large slope failure is observed in the experiment. In Case 4, as well, axial force is mobilized when the flood water head exceeds 1.5 m (after 25 h, see Fig. 4).

When comparing the axial forces in the two cases in Figs. 10 and 11, it can be found that the maximum axial force in Case 4 is smaller than that in Case 3. It should be noted that, in Case 4, the rise in the phreatic surface is not restricted as drainage is not provided. In Case 3, when drainage and reinforcement functions are combined, the maximum axial force recorded near the facing plate is about 4.7 kN. The contribution from the skin friction in the section without the spiral blade is about 2.2 kN, and that from the end reaction is 2.5 kN. In Case 4, the maximum axial force recorded near the facing plate is about 2.2 kN, which is mostly due to the contribution from the skin friction and a negligible amount from the end reaction. The maximum skin friction is the same for both cases.

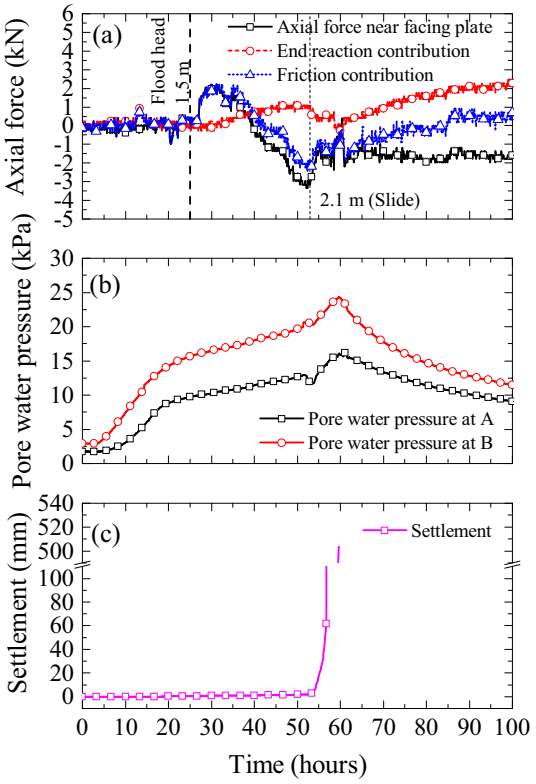

Fig. 11. Time histories of (a) Axial force with its component (b) pore water pressure at location A and B (d) settlement at location F, in Case 4.

The end reaction contribution, however, varies significantly among the cases. The larger end reaction is mobilized when pipes with the drainage function are provided.

The absence of the drainage function in Case 4 results in the higher phreatic surface. The increase in the phreatic surface in the slope surface can cause (i) a decrease in the end reaction capacity, which is mostly related to the rise in pore water pressure at location B; (ii) a decrease in the skin friction related to high pore water pressure at location A; and (iii) instability of the slope due to a decrease in soil resistance, which is also related to the pore water pressure at location A. The instability of the slope, in turn, may cause an increase in the end reaction due to the increase in load retained by the pipes. In observing the time histories of the pore water pressure at locations A and B, and the flood water head in the supply tank, the following relations can be observed:

Case 3: Pore water pressure head at location A < Pore water pressure head at location B < Flood water head
Case 4: Pore water pressure head at location A < Pore water pressure head at location B = Flood water head

As explained in (i) above, the presence of a much higher pore water pressure head at location B in Case 4 compared to Case 3 might have resulted in the end reaction not being mobilized adequately in Case 4. Also, in Fig. 11(a), it can

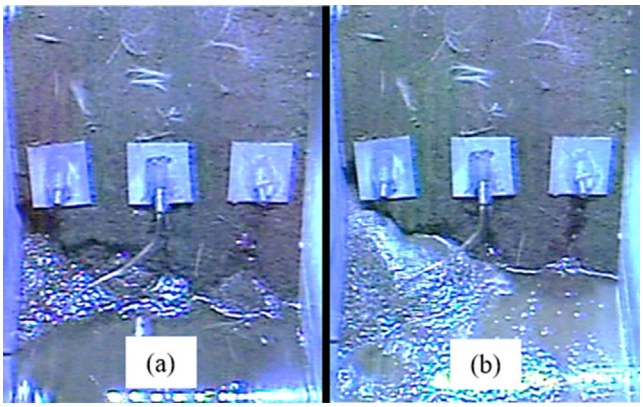

Fig. 12. Erosion of soil near the slope surface in Case 4 (a) at 37 h (b) 52 h of seepage flow.

be observed that there is a reduction in the axial force before the large failure of the slope, i.e., before 53 h of seepage flow, beginning at $t = 40$ h. The axial force decreases and becomes negative, i.e., the tensile force decreases from the initial condition. This negative value for the axial force could be due to the loss of soil mass near the slope surface. A snapshot of the video camera record on the front slope surface, given in Fig. 12, shows the gradual erosion of the soil and the deposition of the eroded soil near the toe of the slope. Fig. 12 shows the start of the erosion of the soil at 37 h and the soil deposited near the toe at 52 h of seepage flow, respectively. The progression of the soil erosion also corresponds to the gradual decrease in axial force in Case 4 and the eventual negative axial force.

The flood-induced bending moment at the different distances from the slope surface along the length of the pipe at the different relevant times are plotted along with the flood-induced soil reactions on the pipe for Cases 3 and 4 in Fig. 13. The soil reaction here is the change in soil pressure in response to the soil movement. The bending moment is measured by the strain gauges placed at four different locations on the pipe surface, as shown earlier in Fig. 2. The embedment length of the pipe is 5.6 m. The section with the spiral blade is from 4.6 m to 5.6 m from the slope surface. Unfortunately, the strain gauges are not attached to the section with the spiral blade. The bending moment is analyzed by taking the start of the seepage flow as a datum, i.e., the bending moment at the onset of seepage flow is set at zero. The bending moment analyzed here is due to the soil mass movement caused by the seepage flow. The soil reaction is calculated from the weighted residual numerical differentiation, as described in Brandenberg et al. (2010). The bending moment data, recorded during the centrifuge experiments, are double differentiated using this method.

From the distributions of the bending moments and the soil reaction in Case 3, it can be observed that with the progression of the seepage flow, fluctuations in the bending moment and the soil reaction are observed, whereas in Case 4, there is minimal change in the soil reaction with the progression of the seepage flow. In Case 3, before the start of the seepage flow, the soil below the pipes erodes

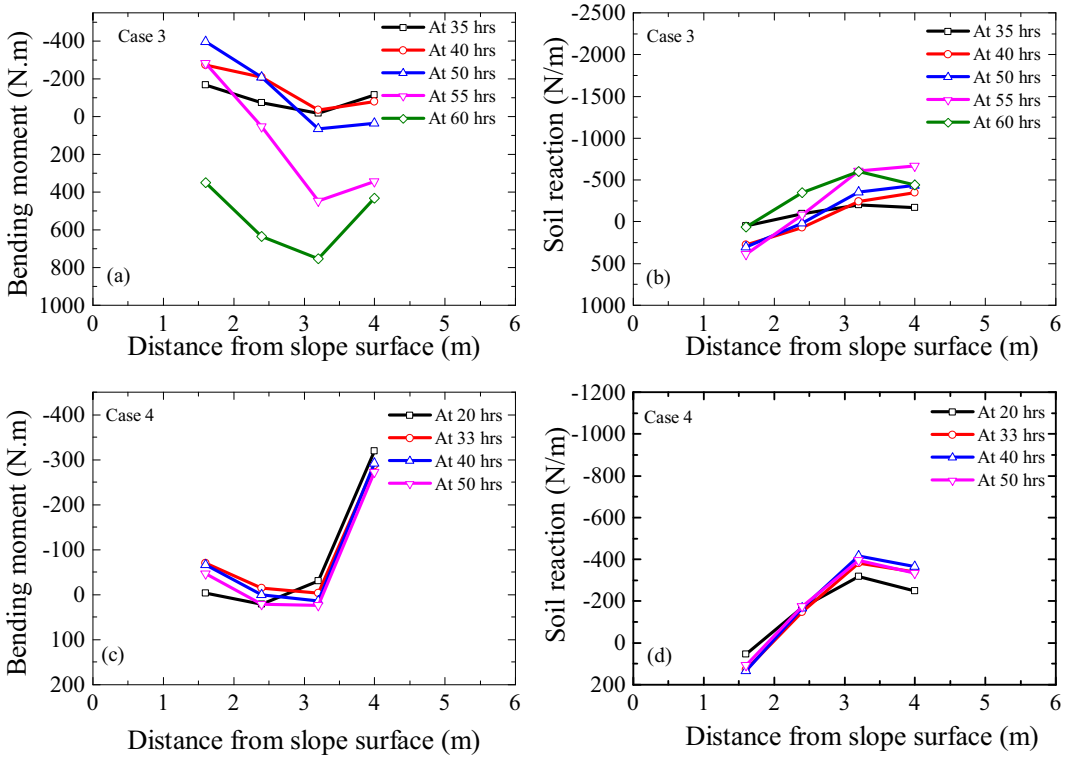

Fig. 13. Bending moment and earth reaction along length of pipe (a) bending moment in Case 3; (b) Soil reaction in Case 3; (c) bending moment in Case 4; (d) earth reaction in Case 4.

near the surface, which might result in the loosening of the soil below the pipe. This loosening of the soil could allow the pipe to move more freely, and hence, bring about more of a change in the soil reaction with the seepage flow. In Case 4, the failure is very sudden, as reflected by the sharp change in settlement in the time history of the settlement seen in Fig. 6. Initially, therefore, when there is a small change in settlement, the bending moment is small which is followed by sudden large deformation (around 55 h of seepage flow), causing the observation of the bending moment to be out of the range.

In either case, the maximum soil reaction is less than 1 kN/m. If it is considered that a possible static load induced by the self-weight of the soil at the middle of the section without the spiral blade is 7.7 kN/m, it can be said that the calculated soil reaction will be minimal. This suggests that the reinforcement contribution is, therefore, predominantly through the mobilization of the axial force and minimally through the bending moment with the specifications of the steel pipes used.

5. Summary and conclusions

This study has investigated the effectiveness of steel drainage pipes which combine drainage and reinforcement functions against the flood-induced deformation of a sand levee with a 1H:1V slope through centrifugal tests. One case of the unreinforced slope and five additional cases of the reinforced slope with varying levels of protection have been studied. The unreinforced slope served as the control for the other cases of the investigation. The contribution of each function of the proposed steel drainage pipes in slope protection was also investigated through the tests.

It was found that with the rise in pore water pressure in a sand levee during a flood, the slope experienced significant deformation when no protection was provided. The slope with the protection exhibited increased resilience against the flood. The protected slope was able to withstand a higher flood water level and a longer flood duration. Moreover, the propagation of the slip surface and deformation was limited. Steel drainage pipes for both drainage and reinforcement functions were found to be more effective than the traditional method of protection using only either the drainage or the reinforcement function. When only drainage or reinforcement is provided as a countermeasure against the seepage flow in a slope, failure will be delayed, although large slope deformation will not be prevented. The drainage function of the steel drainage pipes was seen to limit the rise of the phreatic surface in the levee through the quick drainage of the seepage water from the levee. The drainage of seepage water limited the rise in the pore water pressure, especially near the slope surface. With the specifications of the steel pipes used in the model slope, the reinforcement was predominantly provided through the mobilization of the axial force and very much less through the mobilization of the bending moments that provided additional confinement to the soil in the shallower portion. The mobilization of the axial force was contributed by (i) the end reaction developing due to the portion of the steel pipes with spiral blades and (ii) the skin friction between the soil and the pipes. The end reaction was not adequately mobilized in the pipes without drainage due to the presence of the higher phreatic surface. Thus, larger axial force was seen to mobilize when the steel pipes with both functions were used compared to the pipes with no drainage.

Acknowledgments

The first author would like to gratefully acknowledge the support provided by the Monbukagakusho (Ministry of Education, Culture, Sports, Science, and Technology) scholarship for graduate students. The work presented in this paper is part of the collaborative research with the Nippon Steel & Sumitomo Metal Corporation. Dr. Shinji Taenaka and Mr. Yoshiro Ishihama, of the Nippon Steel & Sumitomo Metal Corporation, are also acknowledged for their helpful discussions and comments.

References

Allersma, H.G., Bartsch, M., 2004. Centrifuge tests on methods stabilizing embankments. Geo Jordan 2004: Advances in Geotechnical Engineering with Emphasis on Dams, Highway Materials, and Soil Improvement, pp. 311–322.

Brandenberg, S.J., Wilson, D.W., Rashid, M.M., 2010. Weighted residual numerical differentiation algorithm applied to experimental bending moment data. J. Geotech. Geoenviron. Eng. 136 (June), 854–863.

Cai, F., Ugai, K., 2003. Reinforcing mechanism of anchors in slopes: a numerical comparison of results of LEM and FEM. Int. J. Numer. Anal. Meth. 27, 549–564.

Cai, F., Ugai, K., Wakai, A., Li, Q., 1998. Effects of horizontal drains on slope stability under rainfall by three-dimensional finite element analysis. Comput. Geotech. 23, 255–275.

Cargill, Kenneth W., Ko, Hon-Yim, 1983. Centrifugal Modeling of Transient Water Flow. Journal of Geotechnical Engineering 109 (4), 536–555. https://doi.org/10.1061/(ASCE)0733-9410(1983)109:4(536).

Chen, C.N., Chen, H.Y., 2016. Distributions of pore water pressure surround a horizontal drain pipe on a retaining wall under steady state condition. J. Mech. 29 (2), 263–272.

Choi, E.C.C., 1984. Seepage around horizontal drains in hill slopes. J. Hydraul. Eng. 109 (10), 1363–1368.

Chu-Agor, M.L., Fox, G.A., Cancienne, R.M., Wilson, G.V., 2008. Seepage caused tension failures and erosion undercutting of hillslopes. J. Hydrol. 359 (3), 247–259.

Ghiassian, H., Ghareh, S., 2008. Stability of sandy slopes under seepage conditions. Landslides 5 (4), 397–406.

Hamdhan, I.N., Schweiger, H.F., 2011. Slope stability analysis of unsaturated soil with fully coupled flow-deformation analysis. Mathematical Geoscience at the Crossroads of Theory and Practice, Salzburg, Austria.

Horikoshi, K., Takahashi, A., 2015. Suffusion-induced change in spatial distribution of fine fractions in embankment subjected to seepage flow. Soils Found. 55 (5), 1293–1304, Elsevier.

Koito, N., Horikoshi, K., Takahashi, A., 2016. Physical modelling of backward erosion piping in foundation beneath levee. 8th International Conference on Scour and Erosion. Taylor and Francis Group, Oxford, UK, pp. 445–451.

Krahn, J., Fredlund, D.G., Klassen, M.J., 1989. Effect of soil suction on slope stability at Notch Hill. Can. Geotech. J. 26 (2), 269–278.

Li, J., Tham, L.G., Junaideen, S.M., Yue, Z.Q., Lee, C.F., 2008. Loose fill slope stabilization with soil nails: full-scale test. J. Geotech. Geoenviron. Eng. 134 (3), 277–288.

Ling, H.I., Wu, M.-H., Leshchinsky, D., Leshchinsky, B., 2009. Centrifuge modeling of slope instability. J. Geotech. Geoenviron. Eng. 135 (6), 758–767.

Mori, T., Tobita, Y., Okimura, T., 2012. The damage to hillside embankments in Sendai city during the 2011 off the Pacific Coast of Tohoku Earthquake. Soils Found. 52 (5), 910–928, Elsevier.

Mori, T., Uzuoka, R., Chiba, T., Kamiya, K., Kazama, M., 2011. Numerical prediction of seepage and seismic behavior of unsaturated fill slope. Soils Found. 51 (6), 1075–1090.

Ng, C.W., Zhan, L.T., Bao, C.G., Fredlund, D.G., Gong, B.W., 2003. Performance of an unsaturated expansive soil slope subjected to artificial rainfall infiltration. Geotechnique 53 (2), 143–157.

Ng, C.W.W., Zhang, L.M., Wang, Y.H., 2006. The effects of soil nails in a dense steep slope subjected to rising groundwater. In: Zhang, Ng, Wang (Eds.), Physical modelling in geotechnics : 6th ICPMG '06. Taylor & Francis, Hong Kong, pp. 397–401.

Polemio, M., Lollino, P., 2011. Failure of infrastructure embankments induced by flooding and seepage: a neglected source of hazard. Nat. Hazards Earth Syst. Sci 11, 3383–3396.

Rahardjo, H., Hritzuk, K.J., Leong, E.C., Rezaur, R.B., 2003. Effectiveness of horizontal drains for slope stability. Eng. Geol. 69, 295–308.

Rahardjo, H., Santoso, V.A., Leong, E.C., Ng, Y.S., Hua, C.J., 2011. Performance of horizontal drains in residual soil slopes. Soils Found. 51 (3), 437–447.

Resnick, G.S., Znidarcic, D., 1990. Centrifugal modelling of drains for slope stabilization. J. Geotech. Eng. 116 (11), 1607–1624.

Rotte, V.M., Viswanadham, B.V.S., 2012. Performance of 2V:1H Slopes with and without Soil-Nails Subjected to Seepage: Centrifuge Study. GeoCongress, ASCE, pp. 643–652.

Saghaee, G., Mousa, A.A., Meguid, M.A., 2016. Experimental evaluation of the performance of earth levees deteriorated by wildlife activities. Acta Geotech. 11, 83–93.

Saghaee, G., Mousa, A.A., Meguid, M.A., 2017. Synthesis of wildlife-triggered failures in earth levees. Can. Geotech. J.

Schnellmann, R., Busslinger, M., Schneider, H.R., Rahardjo, H., 2010. Effect of rising water table in an unsaturated slope. Eng. Geol. 114 (1), 71–83.

Takemura, J., Kondoh, M., Esaki, T., Kouda, M., Kusakabe, O., 1999. Centrifuge model tests on double propped wall excavation in soft clay. Soils Found. 39 (3), 75–87.

Tei, K., Taylor, R.N., Milligan, G.W.E., 1998. Centrifuge model tests of nailed soil slopes. Soils Found. 38 (2), 165–177.

Timpong, S., Itoh, K., Toyosawa, Y., 2007. Geotechnical centrifuge modelling of slope failure induced by groundwater table change. In: Jakeways, Mclnnes, Fairbank, Mathie (Eds.), Landslides and climate change. Taylor & Francis, London, pp. 107–112.

Thusyanthan, N.I., Madabhushi, S.P.G., 2003. Scaling of Seepage Flow Velocity in Centrifuge Models, Geotechnical Group Technical Report, No. 326, University of Cambridge.

Vanapalli, S.K., Fredlund, D.G., Pufahl, D.E., Clifton, A.W., 1996. Model for the prediction of shear strength with respect to soil suction. Can. Geotech. J. 33, 379–392.

Vandamme, J., Zou, Q., 2013. Investigation of slope instability induced by seepage and erosion by a particle method. Comput. Geotech. 48, 9–20.

Wang, G., Sassa, K., 2003. Pore-pressure generation and movement of rainfall-induced landslides: effects of grain size and fine-particle content. Eng. Geol. 69 (1–2), 109–125.

Zhang, J., Pu, J., Zhang, M., Qiu, T., 2001. Model tests by centrifuge of soil nail reinforcements. J. Testing Eval. JTEVA 29 (4), 315–328.

Zhou, Y.D., Cheuk, C.Y., Tham, L.G., 2009. Deformation and crack development of a nailed loose fill slope subjected to water infiltration. Landslides 6, 299–308.